Photoelectron Spectroscopic Imaging and Device Applications of Large-Area Patternable Single-Layer MoS₂ Synthesized by Chemical Vapor Deposition

Woanseo Park,[†] Jaeyoon Baik,[‡] Tae-Young Kim,[†] Kyungjune Cho,[†] Woong-Ki Hong,[§] Hyun-Joon Shin,[‡,⊥] and Takhee Lee[†,*]

[†]Department of Physics and Astronomy and Institute of Applied Physics, Seoul National University, Seoul 151-747, Korea, [‡]Pohang Accelerator Laboratory, Pohang University of Science and Technology, Pohang 790-784, Korea, [§]Jeonju Center, Korea Basic Science Institute, Jeonju, Jeollabuk-do 561-180, Korea, and [⊥]Department of Physics, Pohang University of Science and Technology, Pohang 790-784, Korea

ABSTRACT Molybdenum disulfide (MoS₂) films, which are only a single atomic layer thick, have been synthesized by chemical vapor deposition (CVD) and have gained significant attention due to their band-gap semiconducting properties. However, in order for them to be useful for the fabrication of practical devices, patterning processes that can be used to form specific MoS₂ structures must be integrated with the existing synthetic approaches. Here, we report a method for the synthesis of centimeter-scale, high-quality single-

layer MoS₂ that can be directly patterned during CVD, so that postpatterning processes can be avoided and device fabrication can be streamlined. Utilizing X-ray photoelectron spectroscopic imaging, we characterize the chemical states of these CVD-synthesized single-layer MoS₂ films and demonstrate that the triangular-shaped MoS₂ are single-crystalline single-domain monolayers. We also demonstrate the use of these high-quality and directly patterned MoS₂ films in electronic device applications by fabricating and characterizing field effect transistors.
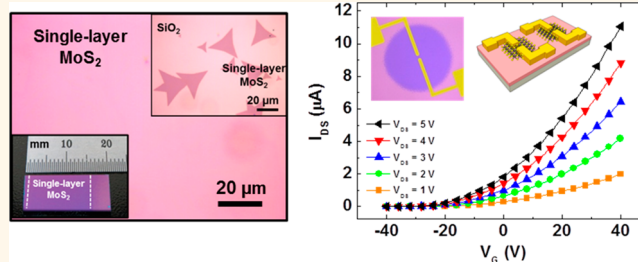
KEYWORDS: transition metal dichalcogenide · molybdenum disulfide · chemical vapor deposition · X-ray photoelectron spectroscopy · field effect transistors

R ecently, molybdenum disulfide (MoS₂), a transition metal dichalcogenide semiconductor, has gained a significant amount of attention due to a great potential for atomic-film electronic and optoelectronic device applications.[1−4] MoS₂ has a layered structure in which the molybdenum atoms are sandwiched between layers of sulfur atoms by covalent bonds. The interaction between adjacent S—Mo—S layers is van der Waals force, so the mechanical exfoliation method can be applied to peel off individual layers.[5−8] More importantly, in contrast to graphene with no band gap, MoS₂ is a semiconductor with a direct band gap of 1.8 eV for a single layer.[9,10] Due to its semiconducting properties, MoS₂ has been used in electronic devices and circuits based on field effect transistors (FETs).[11−16] Recently the chemical vapor deposition (CVD) method has been utilized to synthesize MoS₂ films;[17−20] however, the synthesis of large-scale, high-quality, single-layer MoS₂ films still remains a challenge for practical device development. Despite recent progress, existing synthetic approaches that can be used to fabricate large-area MoS₂ films require additional patterning processes.[21−23] These processes may introduce unintentional contamination from other chemicals. Therefore, it is required to directly synthesize patterned, atomic-layer MoS₂ films by CVD on silicon substrates.

In this study, we report the simple method for the synthesis of large-area, high-quality, single-layer MoS₂ films that can be directly patterned during the synthesis, so
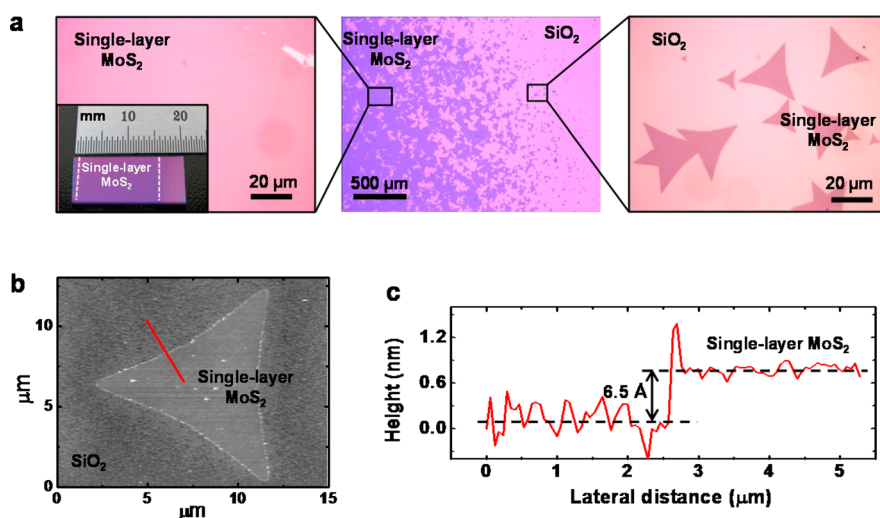
Figure 1. (a) (Left) Optical image of a uniform single-layer MoS$_2$ film on a SiO$_2$/Si substrate. The inset shows a large-scale single-layer MoS$_2$ film at the centimeter scale. (Middle) Optical image of the boundary where the MoS$_2$ film starts to form. The left purple part represents the single-layer MoS$_2$ film. (Right) Optical image of single domains in a triangular-shaped MoS$_2$ film. (b) AFM image showing a MoS$_2$ single domain. (c) Topological cross-sectional profile across the red line indicated in b, displaying the height (0.65 nm) of a single-layer MoS$_2$ film.

that postpatterning processes can be avoided and device fabrication can be made simultaneously. We characterized the synthesized MoS$_2$ films by optical microscopy, Raman spectroscopy, and X-ray photoelectron spectroscopy to represent that large-area, single-layer, and high-quality MoS$_2$ films. We also applied photoelectron spectroscopic imaging to show that the triangular-shaped MoS$_2$ are single-crystalline single domain monolayers, and we successfully demonstrated the field effect transistors made with the high-quality and directly patterned MoS$_2$ films as active channels.

RESULTS AND DISCUSSION

We synthesized the MoS$_2$ films using a chemical vapor deposition system (Teraleader Co., Ltd.). First, SiO$_2$ (270 nm thick)/Si substrates of 20 mm × 20 mm in size were prepared and cleaned in acetone, 2-propanol, and deionized (DI) water for 5 min each. Then, we put MoO$_3$ powder (99.5%, Aldrich) and the substrate covered with a ceramic mask (alumina 99%) on a quartz boat and inserted it into the furnace. Additionally, we put sulfur powder (99.98%, Aldrich) on another quartz boat and placed it on an electric heater. The furnace was heated to ~700 °C, and the electric heater was heated to ~200 °C. The sulfur powder evaporated and flowed into the furnace. This process was continued for 5 min in an atmosphere of Ar (150 sccm) in the furnace. Then, the furnace was allowed to cool in the Ar atmosphere for ~10 h. In this way, MoS$_2$ films that are a single atomic layer thick were synthesized on the substrate. More detailed information on this process is available in the Supporting Information (Figure S1).

Figure 1a shows representative optical images of CVD-synthesized MoS$_2$ films on SiO$_2$/Si substrates. The middle image in Figure 1a is a large-area (~2.5 mm) optical view of a MoS$_2$ film. The right image in Figure 1a is a zoomed-in image that shows where triangular-shaped MoS$_2$ films are starting to form on a substrate. In the optical images, the color contrast can be used to differentiate the MoS$_2$ flakes on the SiO$_2$/Si substrates by their thickness (i.e., the number of atomic layers).[24−26] The color contrast of the MoS$_2$ films in Figure 1a is constant, which suggests that they have uniform thickness. A single-layer MoS$_2$ film on a SiO$_2$/Si substrate 270 nm thick appears as a nearly translucent purple in optical images. We measured the thickness of our CVD-synthesized MoS$_2$ films using an atomic force microscope (AFM) (Park Systems, NX10). Figure 1b shows an AFM image obtained from a triangular-shaped MoS$_2$ flake, and Figure 1c displays the topological cross-sectional profile across the scanned line indicated in Figure 1b (red line). The thickness of the MoS$_2$ film was found to be ~0.65 nm, which corresponds to a single-layer MoS$_2$ sheet.[1] This single-layer MoS$_2$ film was uniformly grown to the centimeter scale (see the inset of the right image in Figure 1a).

Raman spectroscopy is a valuable tool for structural characterization, and it has been widely used to study the vibrational properties of two-dimensional materials and to quantitatively determine their thickness.[27] Figure 2a shows Raman spectroscopic data measured from single-layer and multilayer MoS$_2$ flakes synthesized using CVD. Here, the multilayer MoS$_2$ flakes were grown by intentionally increasing the amount of MoO$_3$ added during the CVD process (see Figure S2 in the Supporting Information). The Raman spectroscopy system used in this study (Horiba Jobin Yvon, T64000) employed a 514.5 nm laser. The Raman spectra of the MoS$_2$ flakes were characterized by two major peaks
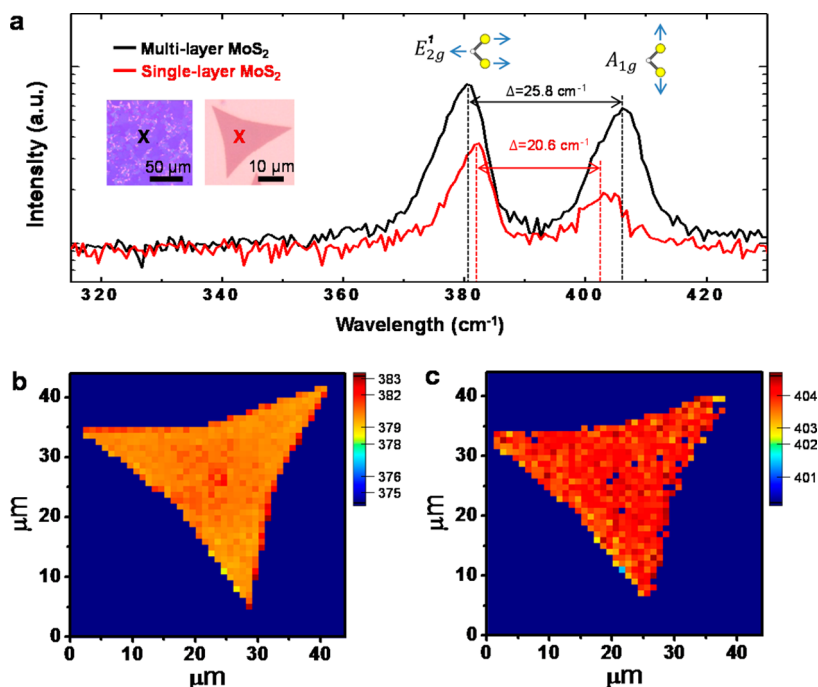
Figure 2. (a) Raman spectroscopy data for single- (red curve) and multilayer (black curve) MoS$_2$ films. The data show the E$^1_{2g}$ and A$_{1g}$ modes at 382.3 and 402.9 cm^{-1}, respectively, for single-layer MoS$_2$ and 380.4 and 406.2 cm^{-1}, respectively, for multilayer MoS$_2$. The insets show optical images of the single- and multilayer MoS$_2$ films with the approximate Raman beam target positions marked. (b, c) Raman spectroscopic images for (b) E$^1_{2g}$ and (c) A$_{1g}$ modes over the area of a single-domain MoS$_2$ film.

centered at 382.3 and 402.9 cm^{-1}. These peaks were assigned as the E$^1_{2g}$ mode (which corresponds to the vibrational motion of Mo and S atoms in the $x-y$ layered plane) and the A$_{1g}$ mode (which corresponds to the vibrational motion of two S atoms along the z-axis of the unit cell) of hexagonal single-crystal MoS$_2$, respectively.[27,28] The exact position of the peaks corresponding to the E$^1_{2g}$ and A$_{1g}$ vibrational modes and the ratio of their intensities depend on the layer thickness of the MoS$_2$ samples. As the thickness of the sample decreased, the frequency of the E$^1_{2g}$ and A$_{1g}$ mode increased and decreased, respectively. These trends can be attributed to Coulombic interactions and to possible stacking-induced changes in intralayer bonding.[29] The Δ value (the peak frequency difference between the E$^1_{2g}$ and A$_{1g}$ modes) was found to be 20.6 cm^{-1}, indicating that the MoS$_2$ film was composed of a single layer (Figure 2a). The Δ value for the multilayer ($\sim$10 layers) MoS$_2$ flake shown in the left inset of the optical image in Figure 2a was found to be 25.8 cm^{-1}. We also did Raman mapping on our CVD-synthesized MoS$_2$ films. Figure 2b and c are the Raman spectroscopic images for the E$^1_{2g}$ and A$_{1g}$ modes, respectively, that were obtained from a single-layer MoS$_2$ flake. The uniform color images in these figures indicate that the CVD-synthesized single-layer MoS$_2$ films have uniform vibrational modes.

We performed X-ray photoelectron spectroscopy (XPS) on CVD-synthesized single-layer MoS$_2$ films to investigate their chemical states (*i.e.*, the existence of

Mo and S in the MoS$_2$ films and the Mo:S ratio (1:2)). The XPS measurements were performed at the 8A1 beamline of the Pohang Accelerator Laboratory, Korea. The photon source was provided by a U6.8 undulator, and the photon energy was set to 690 eV (photon energy resolution $\sim$100 meV). The incident X-ray size was approximately 1 mm $\times$ 1 mm. The X-rays were incident normal to the sample surface, and an electron analyzer (PHI 3057) was positioned at a fixed angle of 54° from the surface normal. This geometry allows sensitive information about the sample surface to be collected using a short probing depth. This setup was ideal for studying the topmost layers of the samples (see Figure S3 in the Supporting Information). Figure 3 compares the XPS spectra obtained from a CVD-synthesized single-layer MoS$_2$ film and a bulk MoS$_2$ single crystal. The binding energies (BE) were calibrated using the Au 4f BE (84 eV) from a nearby mounted gold substrate. As shown in the wide-scan spectra in Figure 3a, the intensity of the S 2p peaks (2p$_{1/2}$, 2p$_{3/2}$) relative to that of the Mo 3d peaks (3d$_{3/2}$, 3d$_{5/2}$) was similar for the MoS$_2$ films and the bulk crystal, suggesting that these CVD-synthesized single-layer MoS$_2$ films and the bulk MoS$_2$ crystal have similar atomic compositions. In addition, the Si 2p peak (positioned at 103.3 eV; consistent with the value for Si in SiO$_2$)[30] was observed for the single-layer MoS$_2$ films, which were grown on a SiO$_2$/Si substrate. The presence of the Si 2p peak can be attributed to the photoelectrons generated from the SiO$_2$ layer underneath the MoS$_2$ layer. The O 1s and C 1s
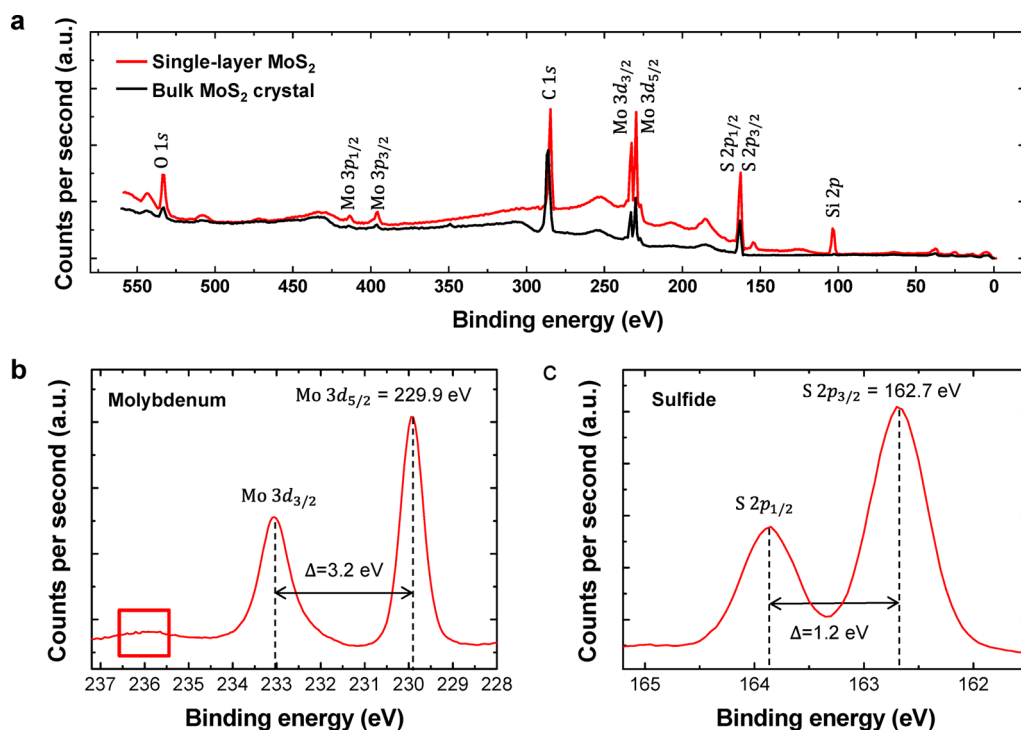
Figure 3. (a) XPS data acquired over a wide range of binding energies (BE) (0−560 eV) from a CVD-synthesized single-layer MoS$_2$ film and a bulk MoS$_2$ crystal. (b) Detailed XPS data from the synthesized MoS$_2$ layer for BEs ranging from 228.0 to 237.2 eV. A peak centered at 236 eV (red box) was not observed, indicating that the Mo in the sample was not oxidized. (c) Detailed XPS data acquired from the MoS$_2$ layer for BEs ranging from 161.5 to 165.2 eV; the sulfide species were examined and oxidation was not observed.

peaks were also observed. The O 1s peak can also be mainly attributed to the photoelectrons from the SiO$_2$ layer. The C 1s peak at 284.8 eV was assigned to adventitious carbons, implying that the MoS$_2$ films or the SiO$_2$/Si substrates can be contaminated with carbon from the ambient air.

High-resolution XPS spectra were obtained for the Mo 3d and S 2p orbitals of a single-layer MoS$_2$ film (Figure 3b and c). The obtained binding energies of the Mo 3d and S 2p orbitals (229.9 and 162.7 eV, respectively) were consistent with previously reported values for the bulk MoS$_2$ single crystal.[31] Note the absence of a prominent peak at ∼236 eV (red box in Figure 3b), which corresponds to the Mo^{6+} 3d$_{3/2}$ orbital, indicating that Mo oxidation is minimal.[32] Similarly, a high binding energy component was not observed between 168 and 170 eV (the S 2p), indicating that the sulfur atoms also are not oxidized. These results suggest that the CVD-synthesized single-layer MoS$_2$ films were composed only of Mo and S species and that they have almost the same stoichiometry as that of the MoS$_2$ bulk single crystal.

In the XPS measurements (Figure 3), the X-ray size at the sample surface was 1 mm × 1 mm. If the film is composed of various material patterns, then XPS mapping must be carried out with an X-ray beam that is smaller than the pattern size. We investigated CVD-synthesized single-layer MoS$_2$ films using scanning photoelectron microscopy (SPEM). SPEM can be used

to map XPS images (Figure 4). The main purpose of the SPEM measurement is to investigate local chemical states with a space resolution of focused X-ray size within the MoS$_2$ layer. By doing this experiment, we can understand if the MoS$_2$ layer is locally contaminated, oxidized, or chemically bonded with other elements.[33] Also, we can obtain thickness homogeneity of the MoS$_2$ layer; for example, one can investigate if the layer is uniformly distributed with a single layer or locally multilayered.[34] This can be achieved by measuring the relative intensity changes of the Mo 3d and S 2p, or of the Si 2p from the substrate.

For the SPEM measurement, an X-ray was focused by an X-ray lens made of a Fresnel zone plate (the focused X-ray size was ∼200 nm × 200 nm) and scanned over the sample area (see Figure S3 in the Supporting Information). The photoelectron detector had 16 channels; at each point (pixel), 16 sets of data were taken simultaneously during scanning. Thus, after a scan, a total of 16 SPEM images with different BE steps were obtained for the sample area. Figure 4a shows SPEM results measured over a 40 μm × 40 μm scan range. MoS$_2$ triangular flakes with a range of BEs from 237.8 eV (far left) to 225.8 eV (far right) were observed, confirming the existence of molybdenum in MoS$_2$. Each channel image was separated by a BE of 0.75 eV. In the individual SPEM images, the intensities of the Mo 3d peaks are high (yellow) and uniform in the regions covered with MoS$_2$; the regions covered with
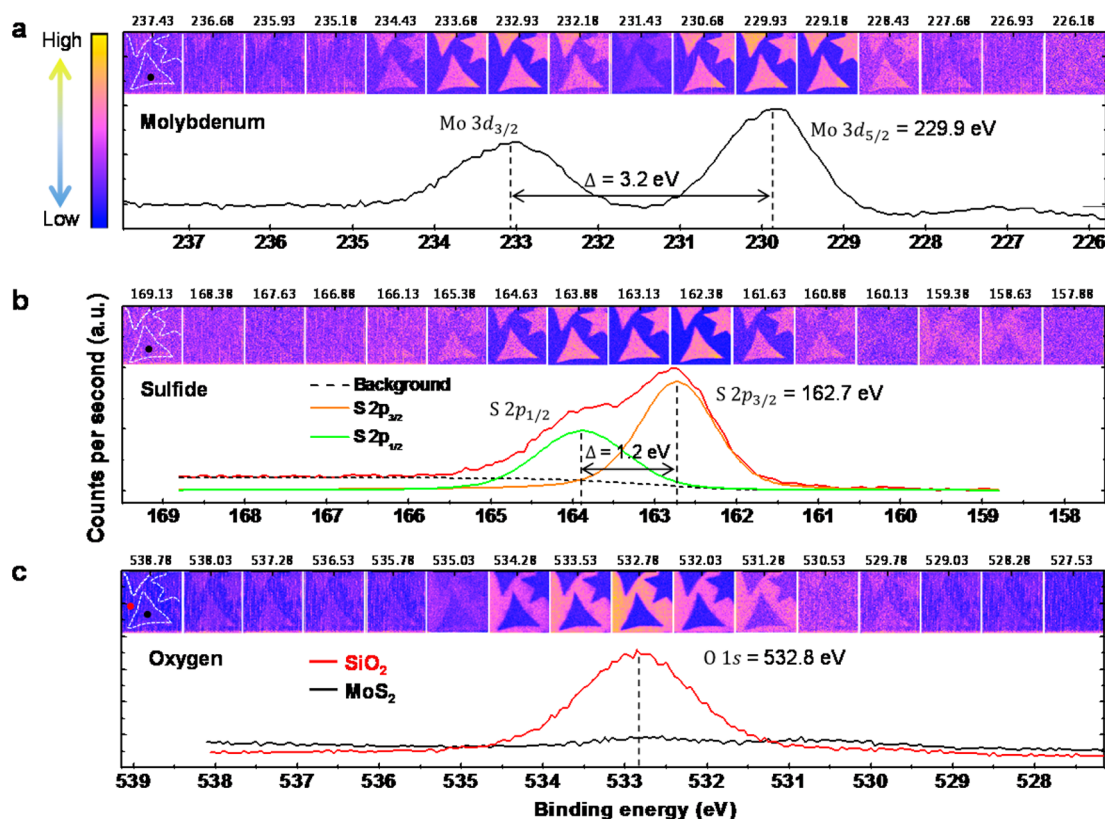
Figure 4. (a) (Upper panel) Scanning photoelectron microscopy (SPEM) images acquired over a single domain, CVD-synthesized MoS_2 film for BEs ranging from 237.8 to 225.8 eV (16 images). The images show the highest contrast at the Mo 3d peak positions [229.9 eV (Mo $3d_{5/2}$) and 233.1 eV (Mo $3d_{3/2}$)]. The region covered with MoS_2 has a high Mo 3d signal intensity (yellow), but the SiO_2 region has a low signal intensity (blue) due to the absence of Mo in that region. White dashed lines, indicative of the MoS_2 region, are marked in the far-left SPEM image. (Bottom panel) XPS data obtained from a point inside the triangular flake (black dot marked in the far-left SPEM image). (b) SPEM images for BEs ranging from 169.5 to 157.5 eV. The SPEM images show the highest contrast in the S 2p region (S $2p_{3/2}$ and S $2p_{1/2}$). The region covered with MoS_2 has high signal intensity (yellow). XPS data were obtained from the same position as above. (c) SPEM images obtained over the O 1s region (BEs ranging from 539.2 to 527.2 eV). The SiO_2 region has high signal intensity (yellow). XPS data were obtained from the black dot in the MoS_2 region and the red dot in the SiO_2 region.

SiO_2 are low in intensity (blue) because Mo is absent (Figure 4a). In particular, the SPEM images in the vicinity of the Mo 3d peaks ($3d_{5/2}$ at ∼229.9 eV and $3d_{3/2}$ at ∼233.1 eV) show clear contrast between the MoS_2 and SiO_2 regions. We chose a particular pixel position (indicated by the black dot in the far-left SPEM image), obtained the XPS spectrum (Figure 4a, main panel), and used this information to estimate the chemical states and the bonding characteristics of the sample. The same XPS result was obtained when an unfocused X-ray was used (Figure 3b). The spectrum was composed of a Mo 3d doublet ($3d_{3/2}$ and $3d_{5/2}$), whose peaks were separated by a binding energy of ∼3.2 eV. Negligible oxidation was observed, indicating that the flake is composed of Mo in a MoS_2 configuration.[35] Furthermore, we can confirm that from the uniform intensity in the image there are no local chemical state changes within the MoS_2 flakes with uniform single-layer thickness.

S 2p SPEM images were also acquired over the same area. S 2p detection was performed between 169.5 (far left) and 157.5 eV (far right) (Figure 4b). The images

exhibited a high and uniform intensity in the MoS_2 area, indicating that the MoS_2 film contains S species and there are no local chemical state changes. Additionally, the XPS spectrum obtained from the position where the black spot is located (Figure 4b, main panel) was composed of a S 2p doublet ($2p_{3/2}$ and $2p_{1/2}$) with a peak separation of 1.2 eV. Again, only negligible oxidation was observed. When O 1s SPEM images were acquired over the same area (ranging from 539.2 eV (far left) to 527.2 eV (far right)), the O 1s contribution measured on the MoS_2 (black curve) was much less than that measured on the SiO_2 (red curve). The image shows contrast opposite that of the Mo 3d and S 2p SPEM images (Figure 4a and b). These SPEM investigations indicate that no local chemical state changes (such as local contamination, local chemical bonding with other elements, locally different oxidation) occurred within the flake and that each flake is uniformly distributed within a single layer of MoS_2.

During the CVD process, MoS_2 films are grown all over the substrate. These films must be properly patterned to form functional device structures. We have
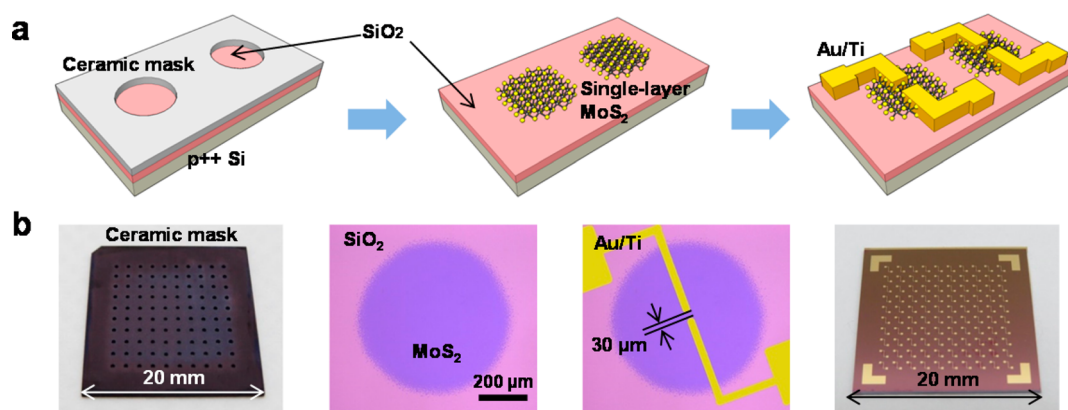
Figure 5. (a) Schematic illustration of the fabrication of MoS_2 FETs made with single-layer MoS_2 films that were directly patterned during the CVD process using a ceramic mask. (b) Optical images of a ceramic mask with circular holes, a circular-shaped single-layer MoS_2 film, a patterned MoS_2 film with Au/Ti (100 nm/5 nm) electrodes, and a completed MoS_2 FET device.
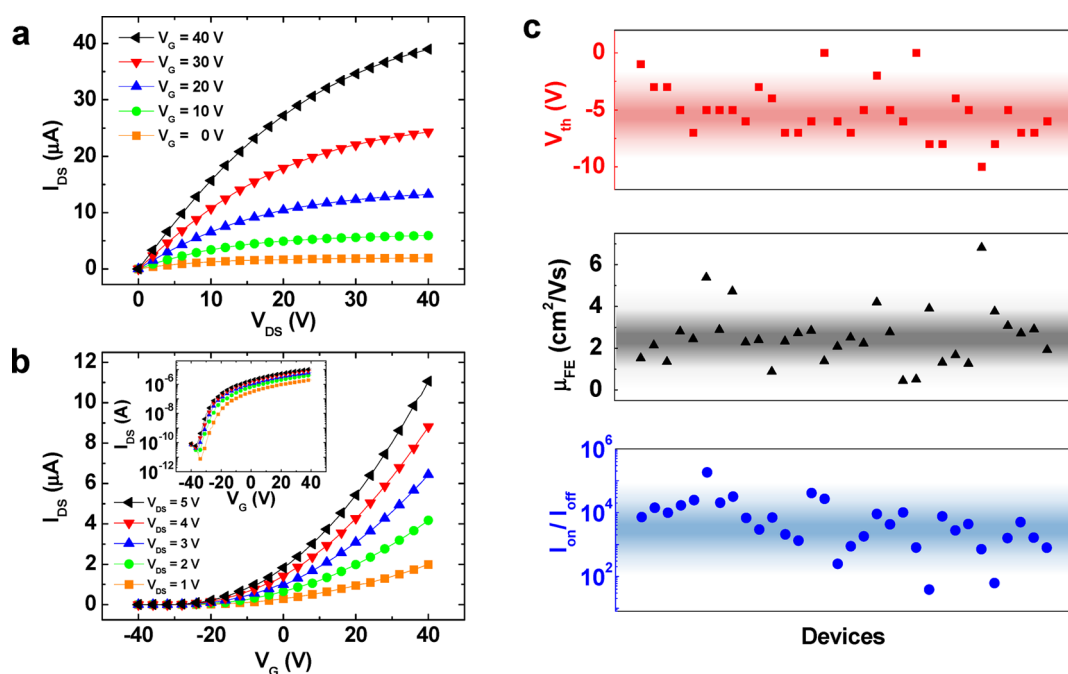
Figure 6. (a) $I_{DS}-V_{DS}$ and (b) $I_{DS}-V_G$ curves for a single-layer MoS_2 FET with semilogarithmic transfer curves (inset). (c) Statistical distribution of the threshold voltages (V_{th}), field-effect mobilities (μ_{FE}), and current on/off ratios (I_{on}/I_{off}) measured from a total of 32 MoS_2 FETs.

developed a novel approach that can be used to directly pattern single-layer MoS_2 films on SiO_2/Si substrates without additional processes. Figure 5a schematically illustrates the process of FET fabrication. First, a 20 mm × 20 mm ceramic mask made of 99.9% alumina was placed on a SiO_2/Si substrate; the mask displayed holes 500 μm in diameter (Figure 5b far-left image). This patterned ceramic mask allows the precursor to access only the substrate exposed by the holes. In this way, MoS_2 films can be grown only in those areas of the substrate (Figure 5a left). We selected a mask made of 99.9% alumina, because this ceramic material is able to endure high temperatures during the CVD process. The synthesized single-layer MoS_2 films were formed in the same shape as the

patterned mask. The diameters of the synthesized MoS_2 films were ~550 μm (Figure 5a middle and Figure 5b second image to the left). Importantly, FET device electrodes can be easily fabricated and defined on these MoS_2 films because they can be grown in well-ordered positions of the substrate. We controllably deposited source and drain electrodes made of Au (100 nm)/Ti (5 nm) layers on these MoS_2 films using an electron-beam evaporator; a shadow mask was aligned over the films (Figure 5a right and Figure 5b second image to the right). The channel was 30 μm in both length and width. This process was used to fabricate complete FET devices on substrates (Figure 5b right).

In addition, we characterized the electrical properties of the FETs that we fabricated from single-layer

MoS$_2$ films. The measurements were performed on a probe station (JANIS model ST-500) using a semiconductor parameter analyzer under vacuum (pressure ~10^{-3} Torr). Figure 6a shows the representative output characteristics (source−drain current *versus* source−drain voltage, I_{DS}−V_{DS}) for different gate voltages ranging from 0 to 40 V at increments of 10 V. The MoS$_2$ FETs exhibited n-type behavior. The devices exhibited ohmic properties at low source−drain voltages, and their currents tended to saturate at high source−drain voltages. The transfer characteristics (source−drain current *versus* gate voltage, I_{DS}−V_G) for different source−drain voltages ranging from 1 to 5 V at increments of 1 V were also investigated (Figure 6b). These data are shown on a semilogarithmic scale in the inset of Figure 6b. Using these transfer characteristics, we can obtain key electrical parameters, such as threshold voltage, current on/off ratio, and field-effect carrier mobility, for the devices. For each device, the threshold voltage was determined by extrapolating the linear portion of the I_{DS}−V_G curve from the point of maximum slope (the point at which the transconductance (dI_{DS}/dV_G) is at a maximum) to the zero drain current.[36] The field-effect mobility was extracted from the following equation: $\mu_{FE} = (dI_{DS}/dV_G)(L/(WC_{ox}V_{DS}))$, where L is the channel length (~30 μm), W is the channel width (~30 μm), and C_{ox} is the gate capacitance, which can be estimated using a parallel capacitor model.[11−13,18,20,37] For the device analyzed in Figure 6a and b, the threshold voltage, current on/off ratio, and field-effect mobility were found to be ~−5 V, 1.83 × 10^5, and 5.4 cm^2/(V s), respectively. Figure 6c shows the statistical distributions of these electrical parameters measured from several devices (32 FETs made with single-layer MoS$_2$ films). The statistical variations of these values can be attributed to the defects and grain boundaries among the active channel MoS$_2$ films.[16] Nevertheless, the electrical performances of FETs made from CVD-synthesized MoS$_2$ films in a back gate structure were comparable with those made from mechanically exfoliated MoS$_2$ films in the similar back gate structure without employing a HfO$_2$ gate dielectric.[1,6,11,12,38]

CONCLUSION

In summary, we developed a novel method to synthesize directly patternable, large-area, high-quality single-layer MoS$_2$ films on SiO$_2$/Si substrates by using patterned ceramic masks during the chemical vapor deposition method. We characterized the CVD-synthesized single-layer MoS$_2$ films by various analytic tools such as optical microscope, AFM, Raman, and XPS. In particular, employing scanning X-ray photoelectron spectroscopy, which can provide valuable information on chemical states by scanning focused X-ray beams on domain-size-specific MoS$_2$ films, we were able to obtain XPS images from single-domain MoS$_2$. We also demonstrated the use of the directly patterned CVD-synthesized MoS$_2$ films in electronic device applications by fabricating and characterizing field effect transistors. The results of this study indicate that large-area, high-quality, single-layer MoS$_2$ films can be synthesized by CVD and directly patterned for atomic-film electronic devices, and it would be worthwhile and interesting to further explore the two-dimensional layered materials and devices.

METHODS

Synthesis of MoS$_2$. The MoS$_2$ films were synthesized using a chemical vapor deposition system (Teraleader Co., Ltd.). First, substrates 20 mm × 20 mm in size (SiO$_2$/Si 270 nm thick) were prepared and cleaned in acetone, 2-propanol, and DI water for 5 min each. Then, the substrates were sonicated in DI water for 15 min. We put MoO$_3$ powder (99.5%, Aldrich) and the substrate covered with a ceramic mask (alumina 99%) on a quartz boat and inserted it into the furnace. Additionally, we put sulfur powder (99.98%, Aldrich) on another quartz boat and placed it on an electric heater (see Figure S1 in the Supporting Information). The furnace was heated to ~700 °C, and the electric heater was heated to ~200 °C. The sulfur powder evaporated and flowed into the furnace. This process was continued for 5 min in an atmosphere of Ar (150 sccm) in the furnace. Then, the furnace was allowed to cool in the Ar atmosphere for ~10 h.

X-ray Photoelectron Spectroscopy and Scanning Photoelectron Microscopy. XPS and SPEM measurements were performed at the 8A1 beamline of the Pohang Accelerator Laboratory, Korea. The photon source was provided by a U6.8 undulator, and the photon energy was set to 690 eV (photon energy resolution ~100 meV). The incident X-ray size was approximately 1 mm × 1 mm for the normal XPS mode (unfocused XPS measurement); the X-ray could be focused to be 200 nm × 200 nm in size using a Fresnel zone plate in the SPEM mode (focused XPS measurement). The X-rays were incident normal to the sample surface, and an electron analyzer (PHI 3057) was positioned at a fixed angle of 54° from the surface normal. This geometry allows sensitive information about the sample surface to be collected using a short probing depth. The photoelectron detector has 16 channels, and in SPEM mode, images can be obtained on all 16 channels simultaneously. Each of the 16 channels can be used to interrogate the sample over a particular binding energy window, and structural information about chemically shifted states can be gleaned from the obtained image. In this study, the defined energy window was 0.75 eV.

Electrical Measurement. I−V measurements (Figure 6) were performed on a probe station (JANIS model ST-500) using a semiconductor parameter analyzer under vacuum (pressure ~10^{-3} Torr).

Conflict of Interest: The authors declare no competing financial interest.

Supporting Information Available: Chemical vapor deposition synthesis of MoS_2 films, multilayer MoS_2 films, XPS, and SPEM, device fabrication of MoS_2 FETs, statistical histograms of V_{th}, μ_{FE}, and I_{on}/I_{off} values for MoS_2 FETs. This material is available free of charge *via* the Internet at http://pubs.acs.org.

REFERENCES AND NOTES

1. Radisavljevic, B.; Radenovic, A.; Brivio, J.; Giacometti, V.; Kis, A. Single-Layer MoS_2 Transistors. *Nat. Nanotechnol.* **2011**, *6*, 147–150.

2. Roy, K.; Padmanabhan, M.; Goswami, S.; Sai, T. P.; Ramalingam, G.; Raghavan, S.; Ghosh, A. Graphene—MoS_2 Hybrid Structures for Multifunctional Photoresponsive Memory Devices. *Nat. Nanotechnol.* **2013**, *8*, 826–830.

3. Esmaeili-Rad, M. R.; Salahuddin, S. High Performance Molybdenum Disulfide Amorphous Silicon Heterojunction Photodetector. *Sci. Rep.* **2013**, *3*, 2345.

4. Lopez-Sanchez, O.; Lembke, D.; Kayci, M.; Radenovic, A.; Kis, A. Ultrasensitive Photodetectors Based on Monolayer MoS_2. *Nat. Nanotechnol.* **2013**, *8*, 497–501.

5. Wang, Q. H.; Kalantar-Zadeh, K.; Kis, A.; Coleman, J. N.; Strano, M. S. Electronics and Optoelectronics of Two-Dimensional Transition Metal Dichalcogenides. *Nat. Nanotechnol.* **2012**, *7*, 699–712.

6. Geim, A. K.; Grigorieva, I. V. Van der Waals Heterostructures. *Nature* **2013**, *499*, 419–425.

7. Chhowalla, M.; Shin, H. S.; Eda, G.; Li, L.-J.; Loh, K. P.; Zhang, H. The Chemistry of Two-Dimensional Layered Transition Metal Dichalcogenide Nanosheets. *Nat. Chem.* **2013**, *5*, 263–275.

8. Butler, S. Z.; Hollen, S. M.; Cao, L.; Cui, Y.; Gupta, J. A.; Gutiérrez, H. R.; Heinz, T. F.; Hong, S. S.; Huang, J.; Ismach, A. F.; *et al.* Progress, Challenges, and Opportunities in Two-Dimensional Materials Beyond Graphene. *ACS Nano* **2013**, *7*, 2898–2926.

9. Mak, K. F.; Lee, C.; Hone, J.; Shan, J.; Heinz, T. F. Atomically Thin MoS_2: A New Direct-Gap Semiconductor. *Phys. Rev. Lett.* **2010**, *105*, 136805.

10. Han, S. W.; Kwon, H.; Kim, S. K.; Ryu, S.; Yun, W. S.; Kim, D. H.; Hwang, J. H.; Kang, J.-S.; Baik, J.; Shin, H. J.; *et al.* Band-Gap Transition Induced by Interlayer van der Waals Interaction in MoS_2. *Phys. Rev. B* **2011**, *84*, 045409.

11. Wang, H.; Yu, L.; Lee, Y.-H.; Shi, Y.; Hsu, A.; Chin, M. L.; Li, L.-J.; Dubey, M.; Kong, J.; Palacios, T. Integrated Circuits Based on Bilayer MoS_2 Transistors. *Nano Lett.* **2012**, *12*, 4674–4680.

12. Pu, J.; Yomogida, Y.; Liu, K.-K.; Li, L.-J.; Iwasa, Y.; Takenobu, T. Highly Flexible MoS_2 Thin-Film Transistors with Ion Gel Dielectrics. *Nano Lett.* **2012**, *12*, 4013–4017.

13. Radisavljevic, B.; Whitwick, B. M.; Kis, A. Integrated Circuits and Logic Operations Based on Single-Layer MoS_2. *ACS Nano* **2011**, *5*, 9934–9938.

14. Bertolazzi, S.; Krasnozhon, D.; Kis, A. Nonvolatile Memory Cells Based on MoS_2/Graphene Heterostructures. *ACS Nano* **2013**, *7*, 3246–3252.

15. Choi, M. S.; Lee, G.-H.; Yu, Y.-J.; Lee, D.-Y.; Lee, S. H.; Kim, P.; Hone, J.; Yoo, W. J. Controlled Charge Trapping by Molybdenum Disulphide and Graphene in Ultrathin Heterostructured Memory Devices. *Nat. Commun.* **2013**, *4*, 1624.

16. Zhu, W.; Low, T.; Lee, Y.-H.; Wang, H.; Farmer, D. B.; Kong, J.; Xia, F.; Avouris, P. Electronic Transport and Device Prospects of Monolayer Molybdenum Disulphide Grown by Chemical Vapour Deposition. *Nat. Commun.* **2014**, *5*, 3087.

17. Shi, Y.; Huang, J.-K.; Jin, L.; Hsu, Y.-T.; Yu, S. F.; Li, L.-J.; Yang, H. Y. Selective Decoration of Au Nanoparticles on Monolayer MoS_2 Single Crystals. *Sci. Rep.* **2013**, *3*, 1839.

18. Najmaei, S.; Liu, Z.; Zhou, W.; Zou, X.; Shi, G.; Lei, S.; Yakobson, B. I.; Idrobo, J.-C.; Ajayan, P. M.; Lou, J. Vapour Phase Growth and Grain Boundary Structure of Molybdenum Disulphide Atomic Layers. *Nat. Mater.* **2013**, *12*, 754–759.

19. Yu, Y.; Li, C.; Liu, Y.; Su, L.; Zhang, Y.; Cao, L. Controlled Scalable Synthesis of Uniform, High-Quality Monolayer and Few-Layer MoS_2 Films. *Sci. Rep.* **2013**, *3*, 1866.

20. van der Zande, A. M.; Huang, P. Y.; Chenet, D. A.; Berkelbach, T. C.; You, Y.; Lee, G.-H.; Heinz, Y. F.; Reichman, D. R.; Muller, D. A.; Hone, J. C. Grains and Grain Boundaries in Highly Crystalline Monolayer Molybdenum Disulphide. *Nat. Mater.* **2013**, *12*, 554–561.

21. Wang, H.; Yu, L.; Lee, Y.-H.; Fang, W.; Hsu, A.; Herring, P.; Chin, M.; Dubey, M.; Li, L.-J.; Kong, J.; *et al.* Large-Scale 2D Electronics Based on Single-Layer MoS_2 Grown by Chemical Vapor Deposition. *IEEE Technol. Dig. IEDM* **2012**, 4.6.1.

22. Levendorf, M. P.; Kim, C.-J.; Brown, L.; Huang, P. Y.; Havener, R. W.; Muller, D. A.; Park, J. Graphene and Boron Nitride Lateral Heterostructures for Atomically Thin Circuitry. *Nature* **2012**, *488*, 627–632.

23. Nam, H.; Wi, S.; Rokni, H.; Chen, M.; Priessnitz, G.; Lu, W.; Liang, X. MoS_2 Transistors Fabricated *via* Plasma-Assisted Nanoprinting of Few-Layer MoS_2 Flakes into Large-Area Arrays. *ACS Nano* **2013**, *7*, 5870–5881.

24. Benameur, M. M.; Radisavljevic, B.; Héron, J. S.; Sahoo, S.; Berger, H.; Kis, A. Visibility of Dichalcogenide Nanolayers. *Nanotechnology* **2011**, *22*, 125706.

25. Li, H.; Lu, G.; Yin, Z.; He, Q.; Li, H.; Zhang, Q.; Zhang, H. Optical Identification of Single- and Few-Layer MoS_2 Sheets. *Small* **2012**, *8*, 682–686.

26. Wang, Y. Y.; Gao, R. X.; Ni, Z. H.; He, H.; Guo, S. P.; Yang, H. P.; Cong, C. X.; Yu, T. Thickness Identification of Two-Dimensional Materials by Optical Imaging. *Nanotechnology* **2012**, *23*, 495713.

27. Ataca, C.; Topsakal, M.; Aktürk, E.; Ciraci, S. A Comparative Study of Lattice Dynamics of Three- and Two-Dimensional MoS_2. *J. Phys. Chem. C* **2011**, *115*, 16354–16361.

28. Frey, G. L.; Tenne, R. Raman and Resonance Raman Investigation of MoS_2 Nanoparticles. *Phys. Rev. B* **1999**, *60*, 2883–2892.

29. Lee, C.; Yan, H.; Brus, L. E.; Heinz, T. F.; Hone, J.; Ryu, S. Anomalous Lattice Vibrations of Single and Few-Layer MoS_2. *ACS Nano* **2010**, *4*, 2695–2700.

30. Jamet, P.; Dimitrijev, S. Physical Properties of N_2O and NO-Nitrided Gate Oxides Grown on 4H SiC. *Appl. Phys. Lett.* **2001**, *79*, 323–325.

31. Eda, G.; Yamaguchi, H.; Voiry, D.; Fujita, T.; Chen, M.; Chhowalla, M. Photoluminescence from Chemically Exfoliated MoS_2. *Nano Lett.* **2011**, *11*, 5111–5116.

32. Zhou, B.; Ceckiewicz, S.; Delmon, B. Synergy in *N*-Ethylformamide Dehydration by Mixtures of MoO_3 and α-Sb_2O_4. *J. Phys. Chem.* **1987**, *91*, 5061–5067.

33. Jeong, H. M.; Lee, J. W.; Shin, W. H.; Choi, Y. J.; Shin, H. J.; Kang, J. K.; Choi, J. W. Nitrogen-Doped Graphene for High-Performance Ultracapacitors and the Importance of Nitrogen-Doped Sites at Basal Planes. *Nano Lett.* **2011**, *11*, 2472–2477.

34. Kim, K.-J.; Lee, H.; Choi, J.-H.; Youn, Y.-S.; Choi, J.; Lee, H.; Kang, T.-H.; Jung, M. C.; Shin, H. J.; Lee, H.-J.; *et al.* Scanning Photoemission Microscopy of Graphene Sheets on SiO_2. *Adv. Mater.* **2008**, *20*, 3589–3591.

35. Lince, J. R. $MoS_{2-x}O_x$ Solid Solutions in Thin Films Produced by RF-Sputter-Deposition. *J. Mater. Res.* **1990**, *5*, 218–222.

36. Arora, N. *MOSFET Models for VLSI Circuit Simulation: Theory And Practice*; Springer-Verlag: New York, 1993.

37. Radisavljevic, B.; Kis, A. Mobility Engineering and a Metal—Insulator Transition in Monolayer MoS_2. *Nat. Mater.* **2013**, *12*, 815–820.

38. Cho, K.; Park, W.; Park, J.; Jeong, H.; Jang, J.; Kim, T.-Y.; Hong, W.-K.; Hong, S.; Lee, T. Electric Stress-Induced Threshold Voltage Instability of Multilayer MoS_2 Field Effect Transistors. *ACS Nano* **2013**, *7*, 7751–7758.